
Article:
Hrabec, A orcid.org/0000-0002-2895-1962, Shahbazi, K orcid.org/0000-0002-1082-4535, Moore, TA orcid.org/0000-0001-6443-2556 et al. (2 more authors) (2019) Tuning spin–orbit torques at magnetic domain walls in epitaxial Pt/Co/Pt1−x Au x trilayers. Nanotechnology, 30 (23). 234003. ISSN 0957-4484

https://doi.org/10.1088/1361-6528/ab087b

Tuning spin-orbit torques at magnetic domain walls in epitaxial Pt/Co/Pt$_{1-x}$Au$_{x}$ trilayers

To cite this article before publication: Ales Hrabec *et al* 2019 *Nanotechnology* in press https://doi.org/10.1088/1361-6528/ab087b

Tuning spin-orbit torques at magnetic domain walls in epitaxial $Pt/Co/Pt_{1-x}Au_x$ trilayers

Aleš Hrabec‡[1], Kowsar Shahbazi[1], Thomas A. Moore[1], Eduardo Martinez[2] and Christopher H. Marrows[1]

[1] School of Physics and Astronomy, University of Leeds, Leeds LS2 9JT, United Kingdom

[2] Departamento Fisica Aplicada, University of Salamanca, Plaza de los Caidos s/n E-37008, Salamanca, Spain

E-mail: c.h.marrows@leeds.ac.uk

E-mail: ales.hrabec@psi.ch

7 February 2019

Abstract. Magnetic domain walls in perpendicularly magnetised thin films are attractive for racetrack memories, but technological progress still requires further reduction of the operationing currents. To efficiently drive these objects by the means of electric current, one has to optimize the damping-like torque which is caused by the spin Hall effect. This not only requires a high net spin Hall angle but also the presence of a Dzyaloshinskii-Moriya interaction (DMI) to produce magnetic textures sensitive to this type of the torque. In this work, we explore the coexistence and importance of these two phenomena in epitaxial $Pt/Co/Pt_{1-x}Au_x$ films in which we control the degree of inversion symmetry-breaking between the two interfaces by varying x. Gold is used as a material with negligible induced magnetic moment and spin Hall effect and the interface between Co/Au as a source of a small DMI. We find no current-induced domain wall motion in the symmetric Pt/Co/Pt ($x = 0$) trilayer. By fitting a one-dimensional model to the domain wall velocity as a function of drive current density and in-plane applied field in samples with non-zero values of x, we find that both net DMI strength and spin Hall angle rise monotonically as Au is introduced. They reach values of 0.75 ± 0.05 mJ/m^2 and 0.10 ± 0.01, respectively, for Pt/Co/Au ($x = 1$).

Keywords: Magnetic multilayer, chiral domain wall, spin-orbit torque, spin Hall effect, Dzyaloshinskii-Moriya interaction

Submitted to: *Nanotechnology*

‡ Present address: Department of Materials, ETH Zürich, 8093 Zürich, Switzerland

1. Introduction

The very first concept of 'racetrack' magnetic recording, based on a soft magnetic ribbon, a writing needle, and a candle, was proposed in 1888 by O. Smith [1]. Today, more a century later, based on the same principle, domain walls (DWs) and skyrmions - the smallest magnetic quasiparticles - are the candidates for magnetic data recording [2, 3] where spin-polarized current flow controls their motion along the racetrack. Although initially it has been suggested that the spin-transfer torque (STT) can drive such non-collinear objects [4, 5], it has been recently revealed that the mechanism describing their interaction with the electric current can be more complex due to spin-orbit torques (SOTs) [6]. Spin-orbitronics is thus a part of spintronics employing the coupling between the electron's spin and its motion to manipulate the magnetic state. Their presence makes the mechanism of magnetization dynamics more complex but also offers more opportunities to enhance the dynamics, when treated properly.

Spin-orbit coupling leads to several phenomena including anisotropic magnetoresistance, magnetocrystalline anisotropy, magnetization damping, anomalous Hall effect, Rashba effect [7, 8], spin Hall effect (SHE) [9], Dresselhaus effect [10] and the Dzyaloshinskii-Moriya interaction (DMI) [11]. Of a particular importance for the DW dynamics is the SHE, which arises from spin-dependent transverse scattering in materials with a large spin-orbit coupling. This drives a transverse spin current that gives rise to a net spin surface accumulation $\sigma \sim \mathbf{J} \times \mathbf{z}$. The ratio of spin accumulation σ to charge current J is typically quantified by the spin Hall angle θ_{SH}. The spin accumulation can diffuse into a ferromagnet and so will exert a torque on a magnetization when a magnetic layer is brought into contact with such a heavy metal. The spin-orbit torque can be, in general, decomposed into two components [12]: $\mathbf{M} \times \sigma$, referred to as a field-like torque, and $\mathbf{M} \times (\mathbf{M} \times \sigma)$, often called a damping-like torque.

Although the field-like torque can, in general, have an impact on the magnetization reversal [13], it has been shown that its impact on the DW dynamics is rather detrimental [14, 15, 16]. Nevertheless, it has been measured to be much smaller than the damping-like torque at a Pt/Co interface [17]. On the other hand, the damping-like torque proved to be extremely useful for driving high-velocity DW motion [18, 19]. Therefore it is the SHE and the associated net spin current flowing into the ferromagnet that predominantly drives the dynamics. The symmetry considerations show that the damping-like torque is relevant only for the motion of Néel DWs in a magnetic layer with perpendicular magnetic anisotropy (PMA) [14, 20] whose presence is not trivial due to their additional magnetostatic energy cost. Néel walls can be stabilized in thin magnetic films by the interfacial Dzyaloshinskii-Moriya interaction (DMI) [21]. The DMI favours cycloidal magnetic structures, such as Néel walls [22, 23] or hedgehog skyrmions [24, 25]. It also imposes a fixed chirality on these structures, which dictates the sign of the damping-like torque inside a Néel DW and therefore the direction of motion with respect to the spin accumulation σ. The heavy metal with high spin-orbit interaction is not only the source of the SHE but serves also as an element breaking the inversion symmetry at the interface between the heavy metal and ferromagnet leading to the presence of interfacial DMI. The coexistence of high SHE and strong DMI paves the path for the possibly most efficient racetrack operation.

The SHE can be maximised by choosing a material with high spin Hall angle such as Pt, Pd, W, or Ta [26] or heavy metal alloys [27, 28], and can be even increased by putting a material with opposite spin Hall angle on the other side of the ferromagnet [29]. As mentioned above, this has to be accompanied by a choice of interface with high DMI and in the case of two interfaces, the two materials can be chosen so that also the DMI is constructively additive [30, 25]. The interface quality has an important impact on SHE due to its transparency for the spin current and also influences the DMI magnitude [30, 31]. To avoid such ambiguities and in order to explore this systematically one has to grow such materials in a controlled way.

While in magnetic semiconductors GaMnAs [32] and in easy-plane ferromagnets Permalloy [33, 34] have been used as model systems to systematically study the relevant torques, the physics of PMA films with broken inversion symmetry at interface is lacking a prototypical system. Ambiguities arising from the quality of the growth prevent an agreement with the theory. Here, we experimentally investigate epitaxial layers of $Pt/Co/Pt_{1-x}Au_x$, shown schematically in figure 1, for which the well-defined crystal lattice and orientation makes the system amenable to treatment by first principles theory. The choice of Au, a heavy element with fully filled $5d$ band, is motivated by a

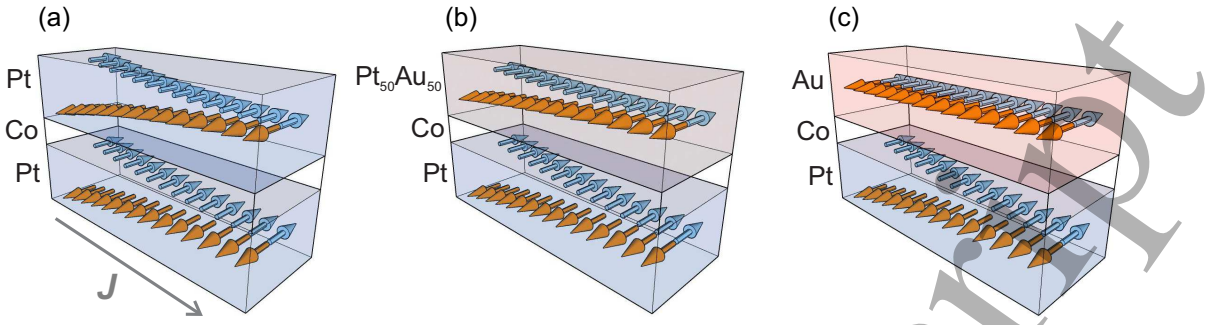

Figure 1. Trilayer stack structures. (a) Pt/Co/Pt ($x = 0$) trilayer. (b) Pt/Co/$Pt_{50}Au_{50}$ ($x = 0.5$) trilayer. (c) Pt/Co/Au ($x = 1$) trilayer. As the Au content in the top layer is increased there is an increasing degree of structural inversion symmetry breaking. Electrons flow in the opposite direction to the conventional current density J. The spin Hall effect in the heavy metal layers converts this into a vertical spin current flow, indicated by the increasing separation of the orange and cyan arrows. In the inversion symmetric Pt/Co/Pt trilayer, equal and opposite spin currents are injected into the Co from above and below, cancelling their effects. The net spin current injected into the Co becomes larger as the inversion asymmetry becomes stronger.

small SHE [35] and a small DMI arising at Co/Au interface [36, 37]. Gold therefore serves as a textbook element giving the opportunity to study the effect of controlled broken symmetry on either side of the ferromagnet and its importance for DMI and SOTs.

2. Epitaxial trilayer growth and characterization

We studied Pt(3 nm)/Co(0.8 nm)/$Pt_{1-x}Au_x$(3 nm) trilayers with $x = 0$, 0.5, and 1 that were prepared by sputtering at high temperatures, as described previously[38, 39]. The main points of the growth method are that a seed Pt layer was sputtered onto a C-plane sapphire substrate at 500°C, followed by Co at a substrate temperature of 100°C. The $Pt_{1-x}Au_x$ layer was grown by co-sputtering from Pt and Au targets at 100°C, with the sputtering powers adjusted to keep the rate $\sim$ 1Å/s. Epitaxial growth along the (111) direction was confirmed by x-ray diffractometry. All the films showed a square hysteresis loop as a function of perpendicular magnetic field in polar Kerr effect measurements, confirming the out-of-plane character of magnetic anisotropy.

The micromagnetic parameters of our trilayers can be established based on our previous detailed characterization of such epitaxial systems. The exchange stiffness $A \approx 20 \pm 1$ pJ/m at this thickness of Co layer [40, 39], whilst the saturation magnetization of the Co layer, once the proximity effects have been accounted for, is $M_S = 1.0 \pm 0.2$ MA/m [39]. The perpendicular magnetic anisotropy, K_u, was previously found to increase as the Au content rises [39], the values for these samples are given in table 1. The domain wall thickness $\Delta = \sqrt{A/K_{\rm eff}}$ is controlled by the effective anisotropy $K_{\rm eff} = K_u - \frac{1}{2}\mu_0 M_S^2$, which includes shape effects, with values again given in table 1. Values for the Gilbert damping coefficient α are taken from prior analysis of field-driven DW dynamics based on micromagnetic simulations incorporating realistic models of disorder [39].

Table 1. Au concentration x, uniaxial anisotropy K_u, DW width Δ, Gilbert damping α, effective DMI constant $D_{\rm eff}$ and effective spin Hall angle $\theta_{\rm SH}$. $D_{\rm eff}$ and $\theta_{\rm eff}$ were extracted from the current-induced DW motion data shown in figures 2 and 3.

x	K_u	Δ	α	D	$\theta_{\rm SH}$
(%)	(MJ/m^3)	(nm)		(mJ/m^2)	
100	0.9 ± 0.2	9 ± 1	0.35 ± 0.05	0.75 ± 0.05	0.10 ± 0.01
50	0.8 ± 0.2	11 ± 2	0.35 ± 0.05	0.22 ± 0.05	0.04 ± 0.01
0	0.7 ± 0.2	17 ± 3	0.17 ± 0.01	0 ± 0.05	0.00 ± 0.01

3. Current-driven domain wall motion measurements

In order to study the efficiency of the SOT, the films were patterned by photolithography and ion beam milling into 2.5 µm wide, 20 µm long wires. The wires were connected to Au contact pads to provide an electrical connection to an external electric circuit, which was impedance-matched to 50 Ω. The DW displacement was observed by wide-field Kerr microscopy at room temperature. The DWs were nucleated and placed into their initial position by the combination of a series of current pulses with an in-plane magnetic field. In the inset of figure 2 we show a differential Kerr micrograph of a typical DW displacement caused by a sequence 2×30 ns long current pulses of density 2.6×10^{12} A/m^2. The DW displacement was measured for various pulse lengths varying between 20 ns and 30 ns to minimize the parasitic effect of the finite rise and fall times.

For each current density the measurement was repeated five times and the average velocity calculated. These average velocities are plotted in figure 2 as a

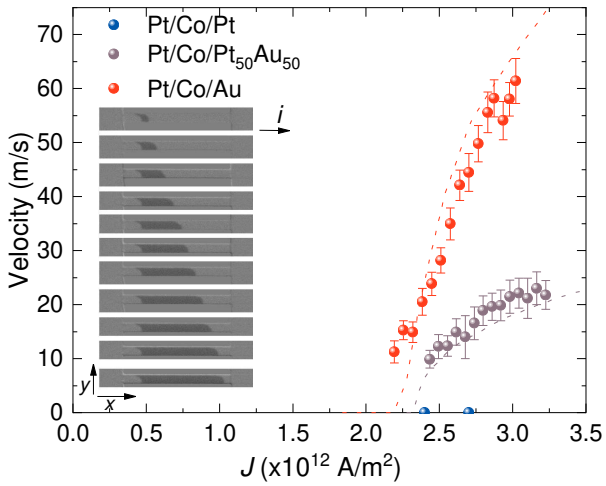

Figure 2. Velocity versus pulse current density for each of the three trilayer stacks. Negligible DW motion was observed for the inversion symmetric Pt/Co/Pt stack. The inset shows a series of differential Kerr images, each taken after application of 2×30 ns, $J = 2.6 \times 10^{12}$ A/m^2 current pulses. The DWs move in the electric current direction. Dashed lines correspond to the results of the simulations based on the 1D model.

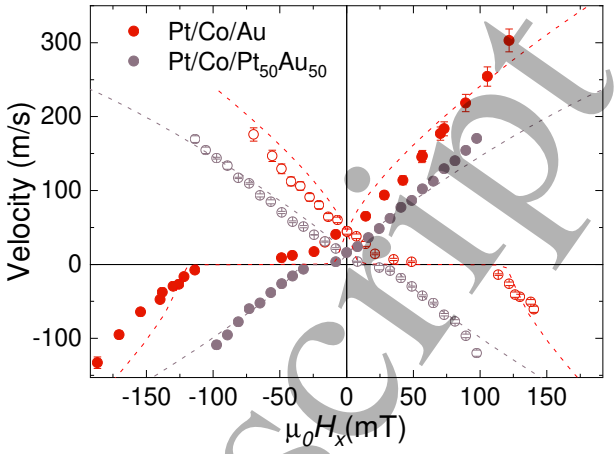

Figure 3. Current induced DW motion in Pt/Co(8 Å)/X as a function of in-plane magnetic field for two different capping layers. The current density is fixed to $J = 2.7 \times 10^{12}$ A/m^2. The full and empty symbols correspond to the down-up and up-down DWs, respectively. The dashed lines correspond to the fit of the results of the 1D model to the data.

function of current density. One can see that the DWs in Pt/Co/Pt ($x = 0$) were almost completely insensitive to the current, which is in accordance with the scenario of compensated spin Hall current coming from the bottom and top layers (figure 1). Note that the current density needed to move the DWs by volume spin-transfer torque is higher than that applied here [41, 42].

The DW velocities in figure 2 are enhanced as soon as the spatial symmetry is broken with addition of Au into the Pt top layer, and are faster for higher x. The DWs always move against the electron flow, which is in contradiction with volume spin-transfer torque scenario [4] indicating that another mechanism plays a more important role. Instead, in the picture of the SOT, the dominating torque arises from SHE-effective field $\mu_0 H_{\mathrm{SHE}}$, which can be expressed as [35, 21]

$$\mu_0 H_{\mathrm{SHE}} = \frac{\hbar \theta_{\mathrm{SH}} J}{2e M_{\mathrm{s}} t_{\mathrm{Co}}} \qquad (1)$$

where J is the charge current density along the x axis, θ_{SH} is the effective spin Hall angle, and t_{Co} is thickness of the Co layer. The effective spin Hall angle represents the net effect of the vertical spin currents being driven into the magnetic layer from the above and below. In the case of $Pt/Co/Pt_{1-x}Au_x$ trilayers the effective spin Hall current is composed of two parts arising from the bottom and top layers [20, 29]. In a naïve picture one can explain this with a reduction of the SHE coming from the top layer due to the negligible SHE of Au [35], as depicted schematically in figure 1. The resulting effective spin Hall angle will become larger with x since the spin-current arising from the bottom Pt layer becomes uncompensated by the top layer. At the same time, with the increased trilayer asymmetry, the effective DMI increases and enforces the chiral Néel wall structure. As a result, higher DW velocities are observed and their direction of motion is in agreement of left-handed DW chirality [43] and positive effective spin Hall angle governed by the Pt layer [44].

In order to get more quantitative insight into this process, the DW velocities were measured as a function of in-plane field $\mu_0 H_x$ applied along the length of the wire for a fixed value of $J = 2.7 \times 10^{12}$ A/m^2. The DW velocities for up-down and down-up DWs as a function of the in-plane field are displayed in figure 3. The DW velocity is zero in a region around a stopping field $\mu_0 H_x = -\mu_0 H_{\mathrm{DMI}}$, where H_{DMI} is the effective field across the DW arising from the DMI [21]. This is when the applied field cancels this effective DMI field, the DW structure reverts to Bloch wall configuration favoured by the magnetostatics, which, as stated above, is insensitive to the SOT. This stopping field is therefore a direct measure of the DMI strength $D = \mu_0 H_{\mathrm{DMI}} M_{\mathrm{s}} \Delta$. The sign of the DW motion is reversed on either side of this field which agrees with the SOT scenario because it is the mutual combination of spin Hall angle and the DW chirality which dictates the direction of the DW motion. The field reverses the DW chirality and so the direction of the DW motion. The velocities are enhanced with the further increase of the in-plane field. The values of D measured from these stopping fields are given in table 1. They are in good agreement with those obtained from asymmetric bubble expansion [39] when the $1/t_{\mathrm{Co}}$ scaling of the interfacial DMI is taken into account.

In order to describe the experimental results of the current-driven DW motion, we have performed simulations based on a 1D model of SOT-driven DW motion [45]. In the simplest version of this model, the DW dynamics is described by two variables: the DW position q, and the internal DW angle ψ defined as the angle between the internal DW moment with respect to the positive longitudinal axis $x > 0$. The model may be extended by introducing a third variable, the DW tilting angle χ, which describe the orientation of the normal unit vector to the DW plane with respect to the $+x$-axis. The corresponding equations, which here were numerically solved using a commercial solver, are presented in detail in reference [45].

In agreement with other observations, the bulk spin transfer torques (STT) were neglected in this analysis. As discussed in the introduction, field-like torques are expected to be small in systems like the one we have studied. We verified that setting the field-like SOT to zero does not modify significantly the presented results in comparison to keeping a field-like torque term of up to one order of magnitude smaller than the damping-like SOT. Hence, for simplicity of calculation, our results were obtained assuming that both volume STT and the field-like SOT are zero. Also, in the light of the above considerations, the damping-like SOT was assumed to be due to the spin Hall effect.

The values of A, K_{u}, M_{S}, α, as described in section 3 above and given in table 1, augmented by the values of D obtained from the stopping field analysis, were used as inputs to the model. The data in figure 2 clearly indicate that there is a pinning threshold for the DW propagation, i.e. there is a minimum current density below which the DWs do not propagate. We therefore introduced an effective pinning field, H_{pin}, opposing the free DW motion, as an extra fitting parameter. This effective pinning field is assumed to be a periodic spatial function $H_{\mathrm{pin}} = \sin(2\pi x/L_{\mathrm{pin}})$, parameterised by the maximum amplitude of the local pinning and the pinning periodicity L_{pin}. We assumed that $L_{\mathrm{pin}} = 2\Delta \approx 20$ nm, consistent with high resolution transmission electron microscopy cross-sectional imaging [39]. The pinning field amplitude was chosen to match the experimental current density threshold in the $v(J)$ curves shown in figure 2. Whilst both the simple and extended models yield very similar results for the $x = 0.5$ trilayer, the additional tilting parameter χ is necessary to properly describe the $x = 1$ trilayer that has higher DMI. Here we show the results of the simple model for the former and those of the extended model for the latter.

The experimental data show low velocity motion for current densities just below the depinning threshold in the model. This is due to thermally-activated current-assisted creep motion [46], which our zero-temperature model is not capable of treating. Although the description of the disorder and pinning by the periodic pinning introduced in the 1D model constitutes an approximation of the real origin of the disorder in these epitaxial stacks (the local variation of the Co thickness), the agreement between the experimental $v(J)$ data (circles in figure 2) and the 1D model predictions (dashed lines) is remarkable for values of J higher then the depinning threshold.

The same inputs were used to simulate the $v(H_x)$ data in figure 3, with the results shown as dashed lines. Again, the agreement is excellent. The sole remaining fitting parameter needed to perform these simulations is the effective spin Hall angle θ_{SH}. The results are shown in table 1, with Pt/Co/Au showing an effective $\theta_{\mathrm{SH}} = 0.10 \pm 0.01$, and $Pt/Co/Pt_{50}Au_{50}$ showing an effective θ_{SH} of about half that value. We assume that Pt/Co/Pt, which does not display any current-driven DW motion, has $\theta_{\mathrm{SH}} \approx 0$.

4. Conclusions

Our results indicate that the effective spin Hall angle θ_{SH} increases roughly in proportion to the Au concentration in the top layer when the bottom Pt layer has fixed thickness and composition, just as the DMI does [39]. This is physically reasonable, since the effective DMI should be negligible in symmetric stacks (Pt/Co/Pt), where the effects at opposite interfaces cancel one another, and the effective DMI parameters should increase with the asymmetry by reducing the Pt concentration (or in other words, increasing the Au concentration) in the top layer. In addition, just as the spin Hall angle of the Au should be also negligible, the effective spin Hall angle in the $Pt/Co/Pt_{1-x}Au_x$ stacks increases with the Au concentration x in the top layer, because again, the effective spin Hall angle becomes null in perfect symmetric stacks (Pt/Co/Pt), where the top and the bottom Pt layers induce opposite spin Hall effects (zero net spin Hall effect). Those predictions are consistent with the fact that no current-driven DW motion was experimentally observed in symmetric Pt/Co/Pt multilayers. We find that the effective SHE increases monotonically with the increased Au content in Pt which can be explained by simple arguments based on asymmetry opening presented in figure 1. However, the origin of the SHE depends on both the intrinsic band structure and extrinsic scattering effects [47], which does not necessarily imply a simple dependence for $\theta_{\mathrm{SH}}(x)$, and first principles studies are needed to properly understand this behaviour. Nevertheless, our findings in these epitaxial trilayers are in qualitative agreement with the previous results obtained for polycrystalline $Pt_{1-x}Au_x$ systems [27, 28].

Acknowledgments

We thank Vincent Jeudy for helpful discussions. This work was supported by the UK EPSRC (grant number EP/I011668/1) and the EU via WALL network (grant number FP7-PEOPLE-2013-ITN 608031). The work by E. M. was supported by Projects MAT2014-52477-C5-4-P and MAT2017-87072-C4-1-P from the Spanish government, and Project No. SA090U16 from the Junta de Castilla y Leon.

ORCID iDs

Aleš Hrabec https://orcid.org/0000-0002-2895-1962
Christopher Marrows https://orcid.org/0000-0003-4812-6393
Eduardo Martinez https://orcid.org/0000-0003-2960-5508
Thomas Moore https://orcid.org/0000-0001-6443-2556
Kowsar Shahbazi https://orcid.org/0000-0002-1082-4535

References

[1] Smith O 1888 *Some possible forms of phonograph* (Electrical World)
[2] Parkin S S P and Yang S H 2015 *Nature Nanotech.* **10** 195
[3] Fert A, Cros V and Sampaio J 2013 *Nature Nanotech.* **8** 152
[4] Li Z and Zhang S 2004 *Phys. Rev. B* **70** 024417
[5] Thiaville A, Nakatani Y, Miltat J and Vernier N 2004 *J. Appl. Phys.* **95** 7049
[6] Manchon A 2014 *Nature Phys.* **10** 340
[7] Bihlmayer G, Koroteev Y M, Echenique P M, Chulkov E V and Blügel S 2006 *Surf. Sci.* **600** 3888
[8] Miron I M, Gaudin G, Auffret S, Rodmacq B, Schuhl A, Pizzini S, Vogel J and Gambardella P 2010 *Nature Mater.* **9**(3) 230
[9] Liu L, Pai C F, Li Y, Tseng H W, Ralph D C and Buhrman R A 2012 *Science* **336** 555
[10] Kurebayashi H, Sinova J, Fang D, Irvine A C, Skinner T D, Wunderlich J, Novák V, Campion R P, Gallagher B L, Vehstedt E K, Zârbo L P, Výborný K, Ferguson A J and Jungwirth T 2014 *Nature Nanotech.* **9** 211
[11] Fert A and Levy P M 1980 *Phys. Rev. Lett.* **44** 1538
[12] Haney P M, Lee H W, Lee K J, Manchon A and Stiles M 2013 *Phys. Rev. B* **88** 214417
[13] Fukami S, Anekawa T, Zhang C and Ohno H 2016 *Nature Nanotech.* **11** 621
[14] Khvalkovskiy A V, Cros V, Apalkov D, Nikitin V, Krounbi M, Zvezdin K A, Anane A, Grollier J and Fert A 2013 *Phys. Rev. B* **87** 020402
[15] Baumgartner M, Garello K, Mendil J, Avci C O, Grimaldi E, Murer C, Feng J, Gabureac M, Stamm C, Acremann Y, Finizio S, Wintz S, Raabe J and Gambardella P 2017 *Nature Nanotech.* **12** 980
[16] Baumgartner M and Gambardella P 2018 *Appl. Phys. Lett.* **113** 242402
[17] Pai C F, Ou Y, Vilela-Leão L H, Ralph D C and Buhrman R A 2015 *Phys. Rev. B* **92** 064426
[18] Ryu K S, Thomas L, Yang S H and Parkin S S P 2013 *Nature Nanotech.* **8** 527–533
[19] Emori S, Bauer U, Ahn S M, Martinez E and Beach G S D 2013 *Nature Mater.* **12** 611–616
[20] Haazen P P J, Murè E, Franken J H, Lavrijsen R, Swagten H J M and Koopmans B 2013 *Nature Mater.* **12** 299
[21] Thiaville A, Rohart S, Jué E, Cros V and Fert A 2012 *Europhys. Lett.* **100** 57002
[22] Benitez M J, Hrabec A, Mihai A P, Moore T A, Burnell G, McGrouther D, Marrows C H and McVitie S 2015 *Nature Commun.* **6** 8957
[23] Tetienne J P, Hingant T, Martínez L J, Rohart S, Thiaville A, Herrera Diez L, Garcia K, Adam J P, Kim J V, Roch J F, Miron I M, Gaudin G, Vila L, Ocker B, Ravelosona D and Jacques V 2015 *Nature Commun.* **6** 6733
[24] Chen G, Mascaraque A, N'Diaye A T and Schmid A K 2015 *Appl. Phys. Lett.* **106** 242404
[25] Moreau-Luchaire C, Moutafis C, Reyren N, Sampaio J, Vaz C A F, Van Horne N, Bouzehouane K, Garcia K, Deranlot C, Warnicke P, Wohlhüter P, George J M, Weigand M, Raabe J, Cros V and Fert A 2016 *Nature Nanotech.* **11** 444
[26] Torrejon J, Kim J, Sinha J, Mitani S, Hayashi M, Yamanouchi M and Ohno H 2014 *Nature Commun.* **5** 4655
[27] Obstbaum M, Decker M, Greitner A K, Haertinger M, Meier T N G, Kronseder M, Chadova K, Wimmer S, Ködderitzsch D, Ebert H and Back C H 2016 *Phys. Rev. Lett.* **117** 167204
[28] Zhu L, Ralph D and Buhrman R A 2018 *Phys. Rev. Applied* **10** 031001
[29] Woo S, Mann M, Tan A J, Caretta L and Beach G S D 2014 *Appl. Phys. Lett.* **105** 212404
[30] Hrabec A, Porter N A, Wells A, Benitez M J, Burnell G, McVitie S, McGrouther D, Moore T A and Marrows C H 2014 *Phys. Rev. B* **90** 020402
[31] Lavrijsen R, Hartmann D M F, van den Brink A, Yin Y, Barcones B, Duine R A, Verheijen M A, Swagten H J M and Koopmans B 2015 *Phys. Rev. B* **91** 104414
[32] De Ranieri E, Roy P E, Fang D, Vehsthedt E K, Irvine A C, Heiss D, Casiraghi A, Campion R P, Gallagher B L, Jungwirth T and Wunderlich J 2013 *Nature Mater.* **12** 808–814
[33] Thomas L, Hayashi M, Jiang X, Moriya R, Rettner C and Parkin S S P 2006 *Nature (London)* **443** 197
[34] Pollard S D, Huang L, Buchanan K S, Arena D A and Zhu Y 2012 *Nature Commun.* **3** 1028
[35] Ryu K S, Yang S H, Thomas L and Parkin S S P 2014 *Nature Commun.* **5** 3910
[36] Kashid V, Schena T, Zimmermann B, Mokrousov Y, Blügel S, Shah V and Salunke H G 2014 *Phys. Rev. B* **90** 054412
[37] Yang H, Thiaville A, Rohart S, Fert A and Chshiev M 2015 *Phys. Rev. Lett.* **115** 267210
[38] Mihai A P, Whiteside A L, Canwell E J, Marrows C H, Benitez M J, McGrouther D, McVitie S, McFadzean S and Moore T A 2013 *Appl. Phys. Lett.* **103** 262401
[39] Shahbazi K, Hrabec A, Moretti S, Ward M B, Moore T A, Jeudy V, Martinez E and Marrows C H 2019 *Phys. Rev. B* **98** 214413
[40] Shepley P M, Tunnicliffe H, Shahbazi K, Burnell G and Moore T A 2018 *Phys. Rev. B* **97** 134417
[41] Cormier M, Mougin A, Ferré J, Thiaville A, Charpentier N, Piéchon F, Weil R, Baltz V and Rodmacq B 2010 *Phys. Rev. B* **81** 024407
[42] Miron I, Zermatten P J, Gaudin G, Auffret S, Rodmacq B and Schuhl A 2009 *Phys. Rev. Lett.* **102** 137202
[43] Belabbes A, Bihlmayer G, Bechstedt F, Blügel S and Manchon A 2016 *Phys. Rev. Lett.* **117** 247202
[44] Nguyen M H, Ralph D C and Buhrman R A 2016 *Phys. Rev. Lett.* **116** 126601
[45] Martinez E, Emori S, Perez N, Torres L and Beach G S D 2014 *J. Appl. Phys.* **115** 213909
[46] San Emeterio Alvarez L, Wang K Y, Lepadatu S, Landi S, Bending S J and Marrows C H 2010 *Phys. Rev. Lett.* **104**

137205
[47] Nagaosa N, Sinova J, Onoda S, MacDonald A and Ong N 2010 *Reviews of Modern Physics* **82** 1539